PAPER

Multimetallic catalysts of RuO$_2$–CuO–Cs$_2$O–TiO$_2$/SiO$_2$ for direct gas-phase epoxidation of propylene to propylene oxide†

T. Chukeaw,[a] A. Seubsai,*[ab] P. Phon-in,[a] K. Charoen,[a] T. Witoon,[a] W. Donphai,[ac] P. Parpainainar,[a] M. Chareonpanich,[ac] D. Noon,[d] B. Zohour[d] and S. Senkan[d]

RuO$_2$–CuO/SiO$_2$ catalysts doped with Cs$_2$O and TiO$_2$ were investigated for the direct gas phase epoxidation of propylene to propylene oxide (PO) using molecular oxygen under atmospheric pressure. The optimal catalyst was achieved at Ru/Cu/Cs/Ti = 8.3/4.2/0.6/0.8 by weight and total metal loading of 21 wt% on SiO$_2$ support. NH$_3$ and CO$_2$ temperature programmed desorption measurements of RuO$_2$–CuO/SiO$_2$ catalyst modified with Cs$_2$O showed that the surface's acidity decreased, resulting in enhanced PO selectivity. The addition of TiO$_2$ increased the PO formation rate by promoting the synergy effect between RuO$_2$ and CuO. Using the Box–Behnken design of experiments on the RuO$_2$–CuO–Cs$_2$O–TiO$_2$/SiO$_2$ catalyst, an extraordinarily high optimal PO formation rate of 3015 g$_{PO}$ h^{-1} kg$_{cat}$$^{-1}$ was obtained with a feed comprised of O$_2$/C$_3$H$_6$ at a volume ratio of 3.1 and (O$_2$ + C$_3$H$_6$)/He at a volume ratio of 0.26, all at 272 °C and 34 cm^3 min^{-1}. To the knowledge of the authors, this is the highest PO formation rate ever reported for direct propylene epoxidation *via* O$_2$.

Introduction

Propylene oxide (PO) is one of the most important feedstocks used in the production of numerous commercial products.[1] Global PO production is approximately 7.5 million tons per year[2] and is forecast to grow at a rate of about 4.2% per year between 2015 and 2020.[3] Currently, the chlorohydrin and hydroperoxide processes are the two major industrial technologies used for PO manufacture. The latter can be divided into two main routes: co-product and hydrogen peroxide to propylene oxide (HPPO). All have major pitfalls. For example, the chlorohydrin and co-product routes, respectively, produce byproducts that are environmentally hazardous (*e.g.* 1,2-dichloropropane) and of less economic value (*e.g.* styrene or *tert*-butyl alcohol) compared to PO. For HPPO, the costly production or acquisition of H$_2$O$_2$ is still a major drawback.[1] Thus, in the past several years, research regarding PO synthesis has been focused on the direct gas-phase epoxidation of propylene with molecular oxygen by using heterogeneous catalysts (C$_3$H$_6$ + 1/2O$_2$ → C$_3$H$_6$O). In the typical mechanism of PO generation, O$_2$ first chemisorbs onto a solid catalyst's active center then dissociates to generate an adsorbed oxygen species (O$_a$) which subsequently reacts with propylene to form relevant intermediates such as allyl radicals, oxametallocycle, and other intermediates. The key in this process is to use a catalyst suitable for the generation of the oxametallocycle that will, in turn, form the PO product. The other intermediates mostly undergo further combustion, *i.e.* producing CO$_2$ and H$_2$O.[1,4] However, the search for a catalyst capable of sustainable industrial-scale PO production (*i.e.* >70% PO selectivity with 10% propylene conversion)[4] has been challenging due to the fact that the current state-of-the-art catalysts have one or more of the following shortcomings: high PO selectivity but low propylene conversion or *vice versa*,[5] low stability,[6,7] and/or the need for a costly additional co-feed (*e.g.* NO$_x$, H$_2$).[8]

Ag-based catalysts were first investigated because they were highly effective for the epoxidation of ethylene.[1] However, partial combustion preferentially takes place when applied to propylene epoxidation due to the abstraction of an allylic hydrogen from C$_3$H$_6$ by an adsorbed neighboring oxygen on the Ag surface.[1,9] Cu-based catalysts for the epoxidation of propylene have been the focus of current research since Cu was found to be a much more intrinsically selective epoxidation catalyst for alkenes containing allylic hydrogens than Ag.[10] This is because the adsorbed oxygen atoms on Cu surfaces have low basicity.[11,12] So the adsorbed oxygen atoms favor interaction with the pi-bond of propylene molecules and form oxametallocycle to create PO molecules. Bi-, tri-, or multi-metallic

[a]Department of Chemical Engineering, Faculty of Engineering, Kasetsart University, Bangkok, 10900, Thailand. E-mail: fengasn@ku.ac.th

[b]Center for Advanced Studies in Industrial Technology and Faculty of Engineering, Kasetsart University, Bangkok, 10900, Thailand

[c]NANOTEC Center for Nanoscale Materials Design for Green Nanotechnology, Kasetsart University, Bangkok, 10900, Thailand

[d]Department of Chemical and Biomolecular Engineering, University of California Los Angeles, CA, 90095, USA

† Electronic supplementary information (ESI) available. See DOI: 10.1039/c6ra12559j

catalysts of Cu have been reported in the most recent studies due to the coexistence of distinct additional solid phase imparting synergistic effects. Examples include: Ag–Cu/BaCO₃,[13] RuO₂–CuO–NaCl/SiO₂,[14,15] SnO₂–CuO–NaCl/SiO₂,[16] Sb₂O₃–CuO–NaCl/SiO₂,[17] Cs⁺–CuOₓ/SiO₂,[18] Ti-modified Cu₂O,[19] etc.[7,20–23] Crystalline CuOₓ was suggested to play the key role in the epoxidation of propylene while the co-component provides a surface for dissociative O₂ adsorption and subsequent surface migration to CuOₓ for PO synthesis.[24] Also, the addition of a combustion-inhibiting alkaline or alkali earth metal ion or ionic compound as a promoter, such as K⁺,[22] Cs⁺,[18] NaCl,[7] and KAc,[23] etc., has been found to improve PO selectivity and/or the PO formation rate by: changing electronic properties of the lattice oxygen to become electrophilic,[20] reducing the acidity of the active surface,[18] or lowering the activation energy for the overall consumption rate.[25] In general, Cu-based catalysts gave 19–58% PO selectivity and ~1–20% propylene conversion.[14,16,17,21,22,26] To date, the highest PO formation rate among Cu-based catalysts in the epoxidation of propylene was obtained from RuO₂–CuO–NaCl/SiO₂ at 40–50% of PO selectivities and 10–20% propylene conversions, representing 153 g_{PO} h^{-1} kg_{cat}^{-1}, between 240 and 270 °C at atmospheric pressure.

In this work, we report an attempt to increase PO formation rate of the previously discovered RuO₂–CuO–NaCl/SiO₂ catalyst. The modification of the main active RuO₂–CuO/SiO₂ component by adding Cs₂O and TiO₂ has been found to significantly enhance the epoxidation of propylene to PO by several-fold. The Box–Behnken design of experiments methodology was used to ascertain the operating conditions-namely temperature, flow rate, and feed composition-under which PO synthesis could be maximized.

Experimental section

Catalysts preparation

All catalysts were prepared by co-impregnation. In a typical synthesis, the catalysts presented in each figure or table were prepared in parallel by mixing appropriate aqueous metal salt precursor solutions of Ru [RuCl₃·xH₂O, Ru 38% min, Alfa Aesar], Cu [Cu(NO₃)₂·3H₂O, Ajax], Cs [CsNO₃, Sigma-aldrich], Ti [titanium plasma standard solution, Ti 1000 µg ml⁻¹, Alfa Aesar], and/or Na [NaNO₃, Alfa Aesar] with the SiO₂ support [Alfa Aesar, surface area of 89.59 m^2 g^{-1}]. The precursor solution volumes and support weights were varied to achieve catalysts comprising a comprehensive set of weight metal ratios and metal loadings. The mixture was stirred at room temperature for 4 h, then stirred at 165 °C until dry, and calcined at 480 °C for 8 h in air.

Catalytic performance evaluation

The propylene epoxidation performance of each catalyst was examined in a traditional packed bed reactor. A prepared catalyst (1.5 mg) was packed in a quartz tube (0.5 cm in diameter) and sandwiched between two quartz wools. The reactant gases were O₂ (Praxair, 99.999%) and C₃H₆ (Linde, 99.5%), along with He (Praxair, 99.999%) as balance gas. In the first step, a volume

ratio of the feed gases was O₂/C₃H₆/He = 2/1/97 at a total flow rate of 50 cm^3 min^{-1} (GHSV = 848 h^{-1}) controlled by using mass flow controllers (KOFLOC 3810 DSII). The reactor temperature was set at 250 °C under atmospheric pressure. In the second step, the Box–Behnken design was applied to determine optimal conditions for obtaining the maximized PO product. Four operating parameters were studied in this work: reaction temperature (190–310 °C), O₂/C₃H₆ volume ratio (0.4–20.0), (O₂ + C₃H₆)/He volume ratio (0.03–0.33), and total feed gas flow rate (30–70 cm^3 min^{-1}). Data analysis was conducted at a pseudo-steady condition (i.e. 0.5–1.0 h after the reactor reached the target temperature) by on-line gas chromatography (Varian CP-4900 Micro GC) with thermal conductivity detector (TCD), Porapak U (10 m) and molecular sieve 5 Å (10 m). The product selectivities and propylene conversions were calculated on the basis of carbon balance,[17] and propylene oxide formation rates were calculated by grams of PO produced per kilogram of catalyst in one hour. Note that, in this work, we have only presented PO and CO₂ products. The CO₂ selectivities and formation rates are not present in all figures. [The CO₂ selectivity for an experiment can be calculated from 100% minus % PO selectivity.] The byproducts (acrolein, acetone, acetaldehyde, etc.) appeared in only trace amounts. The repeatability of all experiments was within ±10%. Tests for the degree of reusability of the catalyst was carried out under the following conditions: reaction temperature of 272 °C, O₂/C₃H₆ volume ratio of 3.1, (O₂ + C₃H₆)/He volume ratio of 0.26, and total feed gas flow rate of 34 cm^3 min^{-1}. 6 runs of 30 min testing were done for the same catalyst, with and without treating with fumed HCl. For the testing without treating with fumed HCl, the catalyst was cooled down to room temperature and left in air for 1 h before starting the new run. For the testing with treating with fumed HCl, after its previous run, the catalyst, still in the quartz tube reactor, was fumed with HCl generated by heating 10 M of HCl at 80 °C in a 2-way glassware connecting to N₂ gas for 1 h. The flow rate of N₂ gas containing HCl was 10 cm^3 min^{-1}.

Catalyst characterization

Powder X-ray diffraction (XRD) patterns were obtained on an X-ray powder diffractometer (XRD: JEOL JDX-3530 and Philips X-Pert) using Cu-Kα radiation, 45 kV and 40 mA to identify crystalline phases. Specific surface area of the SiO₂ support and catalyst was characterized by N₂ physisorption using a Quantachrome Autosorp-1C instrument with BET method at −196 °C. A scanning electron microscope and an energy dispersive X-ray spectrometer (FE-SEM/EDS, FE-SEM: JOEL JSM-7600F) were used to image the catalysts' morphology and elemental composition. X-ray photoelectron spectroscopic studies (XPS, Kratos Axis Ultra DLD) were carried out using Al Kα for the X-ray source to indentify electronic state of the mixing elements. Continuous H₂-temperature programmed reduction (H₂-TPR) measurements were carried out in a continuous-flow Inconel tube reactor held at 25–800 °C with a heating rate of 5 °C min⁻¹. The H₂/Ar mixture gas (9.6% H₂) was introduced into the catalyst bed at total flow rate of 30 cm^3 min^{-1}. The H₂

consumption was continuously monitored using a TCD-equipped GC (Shimadzu GC-2014). Ammonia-temperature programmed desorption (NH_3-TPD, TPD/R/O Thermo Finnigan 1100) and CO_2-programmed desorption (CO_2-TPD, TPD/R/O Thermo Finnigan 1100) techniques were used to analyze the acidity and basicity of catalysts, respectively. For NH_3-TPD, the catalysts were pretreated under He flow at 400 °C for 1 h and cooled down to 40 °C before 10% NH_3/He mixed gas was flowed over the catalysts for 30 min to adsorb on the acid sites. The excess ammonia was eradicated by flowing N_2 at 40 °C for 20 min. The catalysts were then heated to 800 °C at a heating rate of 20 °C min^{-1}, while a flow of He passed over the catalysts at 20 cm^3 min^{-1}. The TPD profiles were detected by a TCD detector and analyzed with a ChemiSoft TPx software. The CO_2-TPD procedure was similar to the NH_3-TPD procedure, except that N_2 was used for the inert gas and that pure CO_2 was flowed over the catalysts to adsorb on basic sites.

Results and discussion

We have previously shown that silica-supported multimetallic RuO_2–CuO–NaCl catalysts exhibit PO selectivities of 40–50% and propylene conversions of 10–20% at 240–270 °C and atmospheric pressure with metal loadings of Ru/Cu/Na = 7.16/3.58/1.79 wt% on the SiO_2 support providing the best performance.[14] Likewise, an early report on the modification of CuO_x/SiO_2 by cesium was found to increase in PO selectivity, similar to the behavior of NaCl in RuO_2–CuO–NaCl/SiO_2 system, by weakening the acidity of the lattice oxygen.[18] Hence, as shown in Fig. 1, we first assessed the catalytic performance of RuO_2–CuO/SiO_2 doped with Cs instead of NaCl. The catalysts were prepared by fixing the weight ratio of Ru/Cu = 7.16/3.58 on SiO_2 with various loadings of Na (Fig. 1a) and Cs (Fig. 1b) at 0.0–4.0 wt% and 0.0–1.0 wt%, respectively. The weight percent range of Cs employed was smaller than that of Na because the atomic size of Cs is larger than Na. Note that Na and Cs will be denoted as NaCl and Cs_2O because of its final form (see XPS spectrum in Fig. 5). In Fig. 1a, the optimum PO formation rate and PO selectivity of NaCl were consistent with the previous findings,[24]

at about 2 wt% loading of Na (490 g_{PO} h^{-1} kg_{cat}^{-1}, 35.4% PO selectivity and 6.0% propylene conversion). Under the same testing conditions the optimum PO formation rate obtained from the Cs loading, as shown in Fig. 1b at 0.6 wt% (533 g_{PO} h^{-1} kg_{cat}^{-1}, 22.6% PO selectivity and 10.7% propylene conversion), was higher than that of the Na loading, indicating that the Cs_2O addition is clearly more effective than the NaCl, even though the PO selectivity of the Cs_2O addition was lower than that of the NaCl addition, if these two promoters were compared in terms of improvement of the catalytic activity for PO synthesis (i.e. PO yield). This could be because, while NaCl is more effective than Cs_2O in reducing acidity of the lattice oxygen which inhibits the CO_2 pathway, it is not as efficient as Cs_2O in enhancing PO production by increasing active sites for PO synthesis (see discussion in Table 1 and Fig. 6). Moreover, excess amounts of Cs_2O, as with the NaCl loading, resulted in decreased PO production. This can be explained in that, at low promoter loading, the promoter species (Cs_2O or NaCl) were expected to be well dispersed, small, and incorporated into the solid structures. They primarily occupy highly acidic sites on the catalyst's surfaces, resulting in the CO_2 suppression and the lower propylene conversions. After all of the highly acidic sites are capped (i.e. passing the optimal PO formation rates), continuously increasing the promoter loadings means that the remaining NaCl or Cs_2O species start to form clusters and segregate from the RuO_2–CuO cluster, resulting in lowering PO selectivities and slightly decreasing propylene conversions due to the larger size of the promoter overlaying the active sites of the RuO_2–CuO clusters.[24]

The main goal of this work was to optimize PO formation rate, therefore the optimal RuO_2–CuO–Cs_2O/SiO_2 catalyst was chosen for further study. Yang and coworkers have found that TiO_x modified on CuO_x can promote PO yield for propylene epoxidation because the surface of Cu–Ti mixed oxides is able to anchor the oxametallocycle, a key intermediate in PO formation.[19] Thus, an attempt to improve the PO production rate of the RuO_2–CuO–Cs_2O/SiO_2 catalyst by adding Ti (denoted as TiO_2) into RuO_2–CuO–Cs_2O/SiO_2 was explored. As indicated in Fig. 2a, increasing the Ti loading from 0.0 to 0.8 wt% resulted in
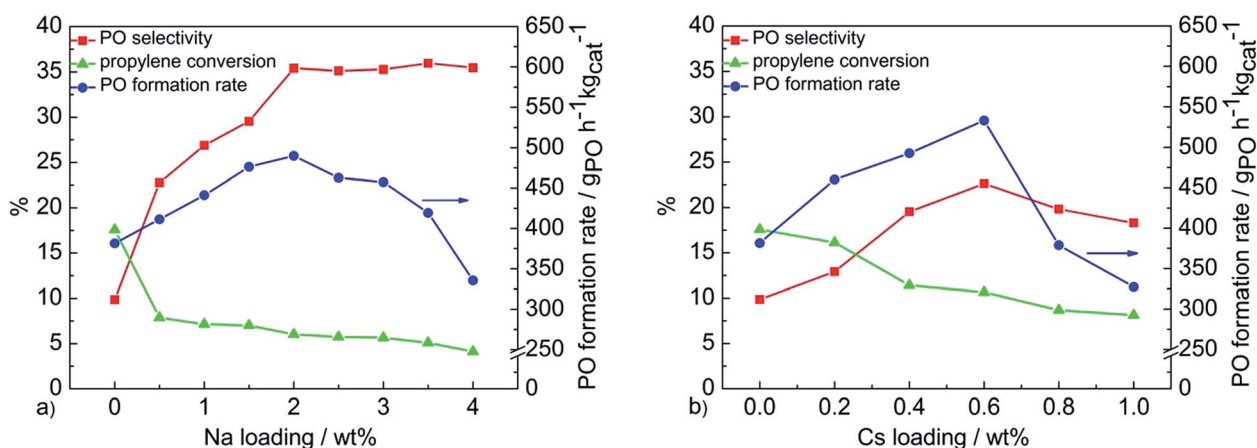

Fig. 1 Catalyst performance of (a) Na at 0.0–4.0 wt% and (b) Cs at 0.0–1.0 wt% loading on Ru–Cu/SiO_2 catalysts (7.16 wt% Ru: 3.57 wt% Cu).

Table 1 Catalyst performance of all combinations of RuO_2, CuO, Cs_2O, and/or TiO_2 on SiO_2. Each catalyst was prepared by fixing wt% of Ru, Cu, Cs, and/or Ti on SiO_2 = 12.59, 6.29, 0.91, 1.21, respectively. The reaction temperature was 250 °C. (AC = acrolein)

Catalyst no.	Catalyst	Selectivity (%)			C_3H_6 conversion (%)	PO yield (%)	PO formation rate (g_{PO} h^{-1} kg_{cat}^{-1})
		PO	AC	CO_2			
1	RuO_2/SiO_2	0.1	1.8	98.1	40.5	0.04	19
2	CuO/SiO_2	18.8	18.8	62.4	0.1	0.02	8
3	Cs_2O/SiO_2	0	35.3	64.7	0.1	0	0
4	TiO_2/SiO_2	0	12.5	87.5	0.1	0	0
5	$RuO_2–CuO/SiO_2$	1.9	0.3	97.8	42.5	0.80	347
6	$RuO_2–Cs_2O/SiO_2$	0.3	0.1	99.6	32.4	0.09	41
7	$RuO_2–TiO_2/SiO_2$	0.2	2.0	97.8	34.6	0.05	22
8	$CuO–Cs_2O/SiO_2$	0	35.3	64.7	0.2	0	0
9	$CuO–TiO_2/SiO_2$	30.0	24.0	46.0	0.1	0.03	14
10	$Cs_2O–TiO_2/SiO_2$	0	0	100.0	0.1	0	0
11	$RuO_2–CuO–Cs_2O/SiO_2$	19.7	0.5	79.8	6.2	1.21	520
12	$RuO_2–CuO–TiO_2/SiO_2$	7.7	0.9	91.4	15.4	1.19	509
13	$RuO_2–Cs_2O–TiO_2/SiO_2$	1.2	1.2	97.6	2.6	0.03	14
14	$CuO–Cs_2O–TiO_2/SiO_2$	0	0	100.0	0.2	0	0
15	$RuO_2–CuO–Cs_2O–TiO_2/SiO_2$	16.8	0.7	82.5	21.0	3.49	801

increase of PO rate to the optimum (from 533 to 601 g_{PO} h^{-1} kg_{cat}^{-1}), then decrease from the optimum at 0.8 wt% of Ti loading to 587 g_{PO} h^{-1} kg_{cat}^{-1} at 1.0 wt% of Ti loading. The PO selectivities minimally decreased from 24.5 to 21.6%, while the propylene conversions slightly increased from 10.6 to 12.5% with increasing Ti loading from 0.0 to 1.0 wt%. The reasons for this will become clear in the discussions of Fig. 6, 7 and Table 1. Furthermore, the addition of Ti from 0.0 to 1.0 wt% into the optimal $RuO_2–CuO–NaCl/SiO_2$ catalyst was also investigated. As shown in Fig. 2b, as the Ti loading increased, the propylene conversion, PO formation rate, and PO selectivity consistently fell, indicating that TiO_2 in the presence of NaCl did not promote the active site. Therefore, the $RuO_2–CuO–NaCl/SiO_2$ catalyst doped with TiO_2 was not studied further. To further optimize the propylene epoxidation performance of RuO_2–$CuO–Cs_2O–TiO_2/SiO_2$, the effects of varying the total metal loading from 5–29 wt%, while fixing the metal ratio at Ru/Cu/ Cs/Ti = 8.3/4.2/0.6/0.8 by weight, was investigated. The results

are shown in Fig. 3a and the XRD spectrum of each catalyst is shown in Fig. 3b. Increasing the loading from 5 to 21 wt% resulted in sharp increases in the PO formation rate, from 187 to 801 g_{PO} h^{-1} kg_{cat}^{-1}, and in propylene conversion, from 3.7 to 20.9%. The PO selectivity gradually decreased from 22.7 to 16.8%. Above 21 wt%, the PO rate and propylene selectivity slightly decreased from 801 to 747 g_{PO} h^{-1} kg_{cat}^{-1} and 16.8–11.5%, respectively; however, the propylene conversion kept increasing to 29.2%. The analyses of the XRD spectra revealed the characteristic diffraction patterns of only RuO_2 ($2\theta = 28.0$, 35.7, 54.2) and CuO ($2\theta = 35.7$, 39.0, 48.8). The characteristic diffraction patterns of Cs_2O and TiO_2 did not appear either because they could be amorphous or because they constituted crystals too small to be detected (<2.0 nm). It can also be seen that the peak intensities for both RuO_2 and CuO crystals increase as total metal loading increases and corresponding PO formation rates increase. This indicates that the existence of crystalline RuO_2 and CuO is crucial for PO formation.[24]
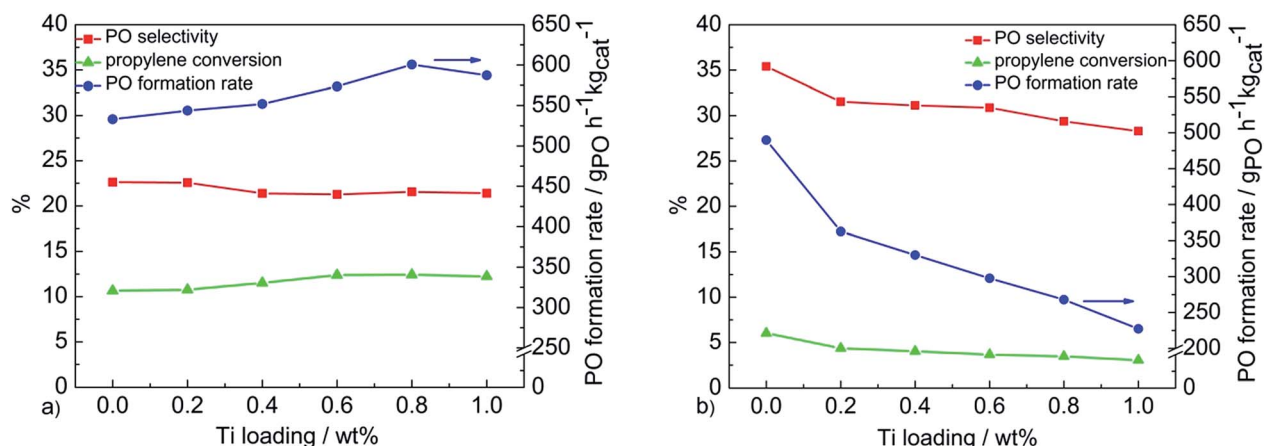

Fig. 2 Catalyst performance of Ti at 0.0–1.0 wt% loading on (a) $RuO_2–CuO–Cs_2O/SiO_2$ catalysts or (b) $RuO_2–CuO–NaCl/SiO_2$ (8.3 wt% Ru: 4.2 wt% Cu: 0.6 wt% Cs or 2.0 wt% Na) at testing temperature of 250 °C.
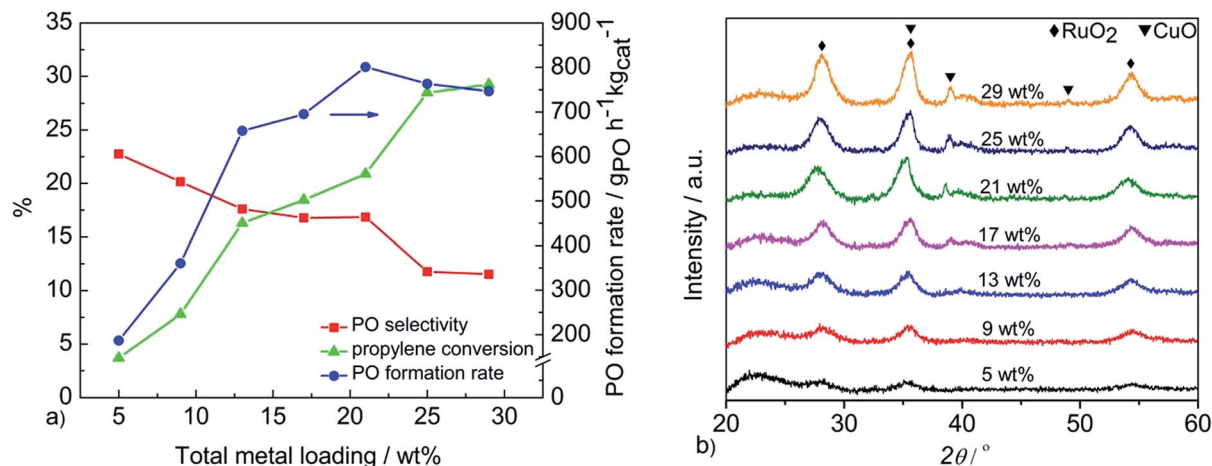
Fig. 3 (a) Various total metal loadings of RuO_2–CuO–Cs_2O–TiO_2 on SiO_2 from 5–30 wt%, Ru/Cu/Cs/Ti = 8.3/4.2/0.6/0.8, and (b) their XRD spectra.

However, the rate of increase in the crystallite sizes could eventually rise to the point at which active sites agglomerate with each other, creating a net decrease in the external surface area available to interact with gases as the loading increases. This plausibly could account for the ultimate fall in the PO formation rate above 21 wt% loading as seen in Fig. 3a.

Fig. 4 shows SEM images and element distributions (Ru, Cu, Cs, and Ti) of the catalysts prepared at different total metal loading. Each metal was uniformly dispersed on the SiO_2 support. Increasing the total metal loading left the particle sizes, approximately 30–50 nm, virtually unchanged. The BET surface area of the optimal catalyst (i.e. 21 wt% loading) was found to be 76.21 m^2 g^{-1} compared to 89.59 m^2 g^{-1} for the unloaded-metal SiO_2 support. The reason for this is that, after the impregnation, the active components were loaded into the SiO_2 support's pores, thus the pore volume decreased, i.e. the surface area decreased.

Fig. 5 shows XPS scanning spectra of Ru, Cu, Cs, and Ti species. The XPS peaks of Ru 3d (Fig. 5a) were Ru $3d_{3/2}$ = 285.1 eV and Ru $3d_{5/2}$ = 281.1 eV, indicating that the resolved binding energy of ruthenium represents the value of RuO_2.[27] Note that the binding energy of C 1s (284.6 eV) also appeared in the Ru region. The binding energies of Cu 2p (Fig. 5b) were Cu $2p_{1/2}$ = 953.2 eV and Cu $2p_{3/2}$ = 933.7 eV, indicating that Cu existed as CuO.[28] The characteristic XPS peaks of Cs 3d appeared at Cs $3d_{3/2}$ = 739.2 eV and Cs $3d_{5/2}$ = 725.2 eV (Fig. 5c), indicating that Cs predominately presents itself in the form of Cs_2O.[29] Furthermore, the binding energies of Ti 2p appeared at Ti $2p_{1/2}$ = 464.1 eV and Ti $2p_{3/2}$ = 458.7 eV (Fig. 5d), confirming that Ti appears in the catalyst as TiO_2.[30] The XPS peak of Ru $3p_{3/2}$ also showed in this region at 463.2 eV. These analyses imply that all four materials are distinct and immiscible, suggesting they contribute some participatory role in the active site for epoxidation when in close proximity.

Table 1 shows the performance of all uni-, bi- and tri-metallic variants of RuO_2, CuO, Cs_2O, and TiO_2, as well as the quaternary RuO_2–CuO–Cs_2O–TiO_2/SiO_2 (15) as the reference catalyst, and reveals the function of each metal. The mono-metallic catalysts no. 1, 3, and 4 were inactive for propylene reactions. RuO_2/SiO_2 (1) typically exhibits a high propylene conversion but a complete combustion is dominant, indicating the absorption of O_2 onto the RuO_2 surface is preferential.[24] CuO/SiO_2 (2) is catalytically active for PO synthesis but the propylene conversion is small, consistent with other reports.[10,24] Bi-metallic catalysts no. 6–8 and 10 produced trace amounts of PO at best, indicating that combinations of RuO_2–Cs_2O, RuO_2–TiO_2, CuO–Cs_2O and Cs_2O–TiO_2 exhibit no synergy. However, RuO_2–CuO/SiO_2 (5) gave a relatively high PO yield and PO formation rate compared to the other bi-metallics, confirming the synergy between RuO_2 and CuO reported earlier.[24] This suggests that an O_2 molecule first adsorbs onto the RuO_2 surface and dissociates into two surface O atoms. The O atoms then migrate across the surface to a neighboring CuO site forming CuO–O. Gas phase propylene then interacts with the CuO–O, ultimately forming the PO via the oxametallocycle. Compared to CuO/SiO_2 (2), the CuO–TiO_2/SiO_2 (9) catalysts presented relatively high PO and AC selectivity but lower CO_2 selectivity and unchanged propylene conversion. This implies that the CO_2 formation route is inhibited by; (1) anchoring the oxametallocycle, thus favoring the generation of PO molecules[19] and/or (2) changing the acidity of the CuO surface (see additional discussion in Fig. 6). Tri-metallic catalyst no. 11 showed the most promising PO selectivity and PO formation rate compared to the other tri-metallics, suggesting that the addition of Cs_2O into RuO_2–CuO can enhance propylene epoxidation to PO by reducing the strong acidity (see discussion in Fig. 6) and increasing the surface active sites for PO formation. The addition of TiO_2 into RuO_2–CuO (catalyst no. 12) also improved either PO rate or PO selectivity but was not as effective as adding Cs at this weight ratio. The tri-metallic catalysts no. 13 and 14, without combination of RuO_2 and CuO, exhibited relatively low to no PO. The most outstanding PO formation rate was achieved from catalyst no. 15. All of these results suggested that RuO_2–CuO/SiO_2 is the main active site for PO generation. Cs_2O and TiO_2 act as promoters to enhance PO formation.

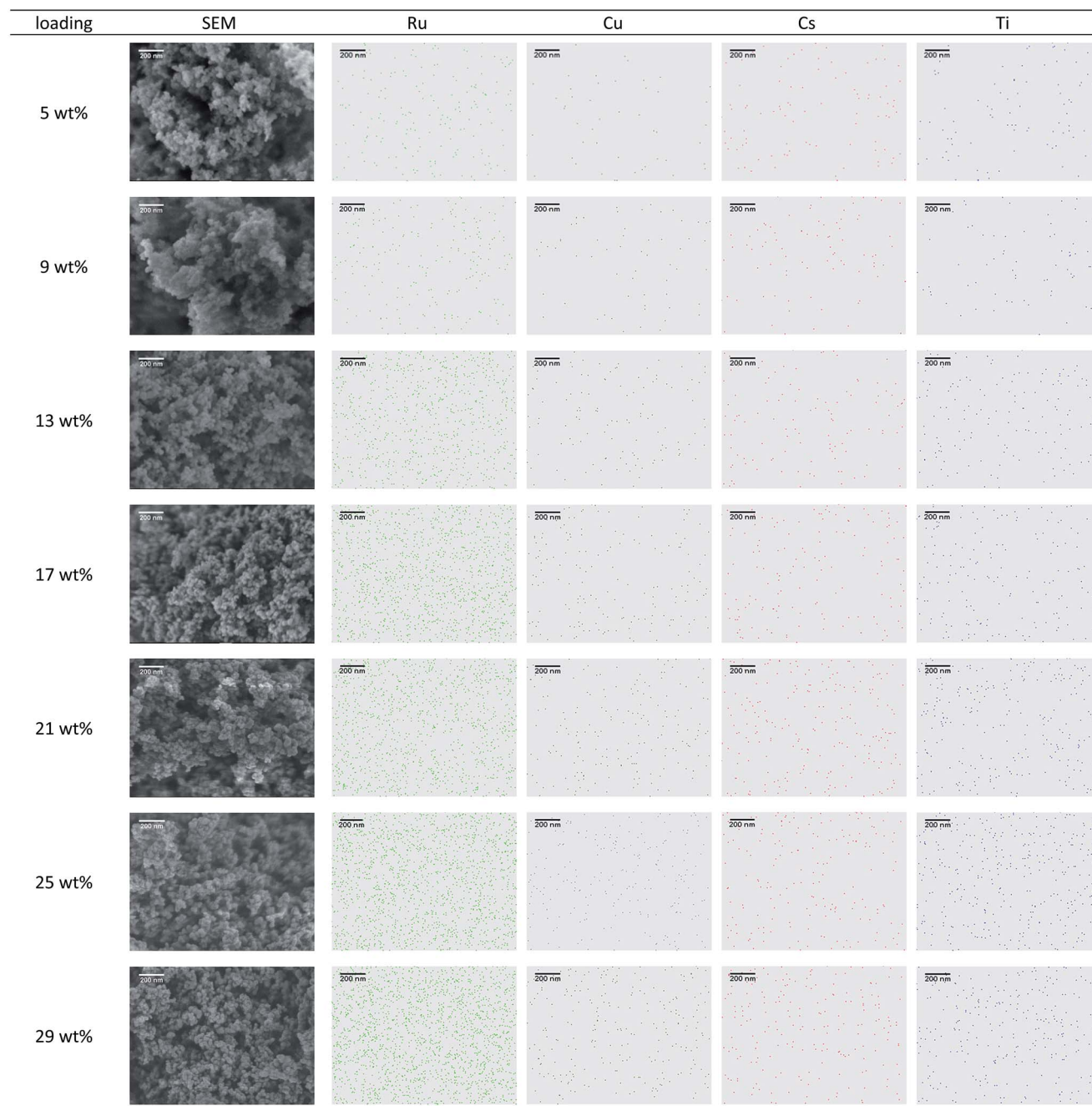| loading	SEM	Ru	Cu	Cs	Ti
5 wt%					
9 wt%					
13 wt%					
17 wt%					
21 wt%					
25 wt%					
29 wt%					

Fig. 4 SEM/EDS of catalysts at 5, 9, 13, 17, 21, 25 and 29 wt% total metal loading on SiO_2, Ru : Cu : Cs : Ti = 8.3/4.2/0.6/0.8. Each scale bar is 200 nm.

Altering the acidity[18,31] and basicity[32] of surfaces has been reported to serve as a useful tool for tuning selectivity. The acidic and basic properties of the RuO_2–CuO/SiO_2, RuO_2–CuO–Cs_2O/SiO_2, and RuO_2–CuO–Cs_2O–TiO_2/SiO_2 catalysts at the optimal weight ratio were assessed using the temperature programmed desorption (TPD) of NH_3 (Fig. 6a) and CO_2 (Fig. 6b), respectively. The re-plots of the performance of RuO_2–CuO/SiO_2 (5), RuO_2–CuO–Cs_2O/SiO_2 (11), and RuO_2–CuO–Cs_2O–TiO_2/SiO_2 (15) catalysts from Table 1 with the acidity and basicity strengths are also presented in Fig. 7. As shown in Fig. 6a, all three catalysts exhibited a similar profile, in which the weak,

medium, and strong acidic sites appeared at approximately 150, 400–500, and 800 °C, respectively. However, the integral peak areas of each site differed slightly among the materials. The addition of Cs_2O to RuO_2–CuO/SiO_2 decreases the peak areas with the medium and strong acidic sites relative to the weak acidic sites. The catalytic activity shown in Fig. 7 indicates that the PO formation rate increased with dramatically decreasing propylene conversion and increasing PO selectivity. This suggests that Cs_2O lessens the presence of high acidity surfaces, thereby inhibiting CO_2 formation in a manner similar to NaCl.[7] This finding is in agreement with He and coworkers' study on
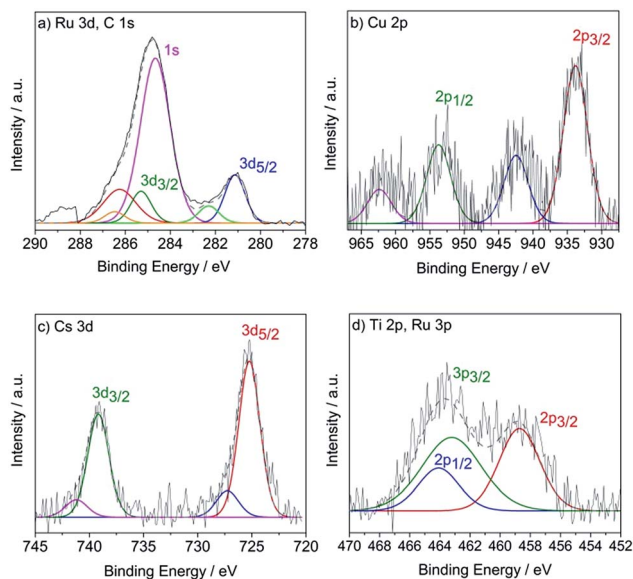
Fig. 5 XPS spectra of RuO$_2$–CuO–Cs$_2$O–TiO$_2$/SiO$_2$ catalyst showing (a) Ru, (b) Cu, (c) Cs, and (d) Ti species; weight ratio of Ru/Cu/Cs/Ti/SiO$_2$ = 12.59/6.29/0.91/1.21/79, total metal loading on SiO$_2$ = 21 wt%. Unidentified peaks are satellite or plasmon peaks.

the modification of Cs$^+$ on CuO$_x$/SiO$_2$.[18] They found that the Cs$^+$ inhibited (1) the isomerization of PO to CO$_2$ because of the weakened acidity of CuO$_x$, thus contributing to the increase in PO selectivity and (2) the reactivity of the lattice oxygen to promote PO production by suppressing the allylic oxidation route of propylene to acrolein and subsequently CO$_2$.

The addition of TiO$_2$ to RuO$_2$–CuO–Cs$_2$O/SiO$_2$ increases the peak area of the strong acidic sites relative to those of the weak and medium sites. This shows that the total number of strong acidic sites has increased again, potentially enhancing CO$_2$ synthesis. However, as indicated in Fig. 7, doping RuO$_2$–CuO–Cs$_2$O/SiO$_2$ with TiO$_2$ significantly improved the propylene conversion and the PO formation rate while leaving the PO selectivity scarcely changed, suggesting the strong acidic site may equally enhance both PO and CO$_2$ formation. This may be because TiO$_2$ itself possesses acidity. Thus, when doping the catalyst with TiO$_2$ the lattice oxygen becomes more electrophilic, increasing the efficiency of the epoxidation of propylene to PO and thereby increasing PO production. Nevertheless, the total oxidation of the generated PO molecules is also likely to take place as the overall acidity increases, thereby increasing the amount of CO$_2$. From all the NH$_3$-TPD results, the overall acidity of the catalysts can be ordered as follow: RuO$_2$–CuO/SiO$_2$ > RuO$_2$–CuO–Cs$_2$O–TiO$_2$/SiO$_2$ > RuO$_2$–CuO–Cs$_2$O/SiO$_2$.

The CO$_2$-TPD results of Fig. 6b and each basic strength related to the performance of each catalyst of Fig. 7 are assessed in a similar manner. The peaks of the weak, medium, and strong basic sites of the catalysts prepared appeared around 110 °C, 590 °C, and 800 °C, respectively. The addition of Cs$_2$O into the RuO$_2$–CuO/SiO$_2$ catalyst increased the total basicity of the catalyst, particularly that of the medium basic site. The strong basic site almost disappeared. Then the addition of TiO$_2$ into
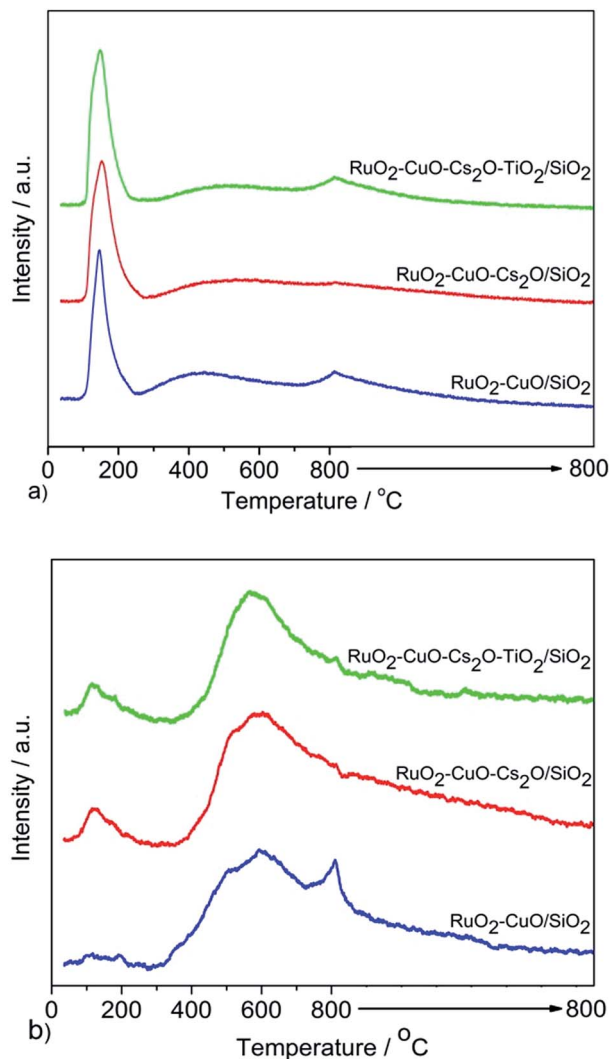

Fig. 6 (a) NH$_3$ and (b) CO$_2$ TPD profiles for RuO$_2$–CuO/SiO$_2$, RuO$_2$–CuO–Cs$_2$O/SiO$_2$, RuO$_2$–CuO–Cs$_2$O–TiO$_2$/SiO$_2$ catalyst. Weight ratio of Ru/Cu/Cs/Ti/SiO$_2$ = 12.59/6.29/0.91/1.21/79, total metal loading on SiO$_2$ = 21 wt%.
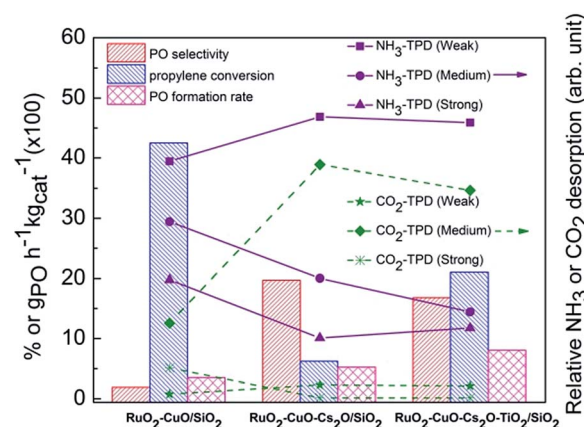

Fig. 7 Relationship between the catalytic performance and acidity/basicity of RuO$_2$–CuO/SiO$_2$, RuO$_2$–CuO–Cs$_2$O/SiO$_2$, RuO$_2$–CuO–Cs$_2$O–TiO$_2$/SiO$_2$ catalysts.

the RuO_2–CuO–Cs_2O/SiO_2 catalyst was found to decrease the catalyst surface's overall basicity, though its basicity remained higher than that of the RuO_2–CuO/SiO_2 catalyst. Thus, the total basicity of the catalysts can be ranked inversely relative to the NH_3-TPD results as follows: RuO_2–CuO–Cs_2O/SiO_2 > RuO_2–CuO–Cs_2O–TiO_2/SiO_2 > RuO_2–CuO/SiO_2. These NH_3- and CO_2-TPD results suggest that an excellent catalyst in the propylene epoxidation should provide not too high acidity or not too high basicity, in other words, intermediate basicity is the key in the search for propylene epoxidation catalysts.[12]

Fig. 8 represents the H_2-TPR spectra of the prepared catalysts. The CuO/SiO_2 catalyst showed a single peak around 290 °C, representing the reduction of bulk CuO consistent with previous reports.[24,33] The single RuO_2/SiO_2 catalyst showed two peaks. The main peak (~175 °C) was attributed to the complete reduction of Ru^{4+} to Ru^0, and the lower temperature peak (~135 °C) was associated with ruthenium species interacting with the support.[34] The Cs_2O and TiO_2 on SiO_2 (not shown here) had no reduction peak observed in this range of temperatures.[35] All combinations of RuO_2 and CuO appeared as a single sharp peak around 170–180 °C, similar to the reduction peaks of the RuO_2/SiO_2 catalyst. Interestingly, the reduction peak of CuO was not observed. This is because of the rapid reduction of CuO induced by a H_2 spillover.[24] In addition, the H_2 consumption spectra of all materials that include at least RuO_2 and CuO together were larger relative to the RuO_2/SiO_2 spectrum, indicating the additional H_2 consumption of CuO. Also, when the CuO or other metal species were added to the catalyst, the shoulder disappeared, either because the peaks were convoluted or because the ruthenium species disappeared. Hence, the reduction of RuO_2 and CuO occurred simultaneously because their nanoparticles were in close contact with each other,[24] consistent with the understood synergy between the two responsible for PO synthesis.

The catalytic performance of these propylene epoxidation catalysts is most heavily influenced by reaction temperature, O_2/C_3H_6 volume ratio, $(O_2 + C_3H_6)$/He volume ratio, and total feed gas flow rate. Investigations of each of these operating
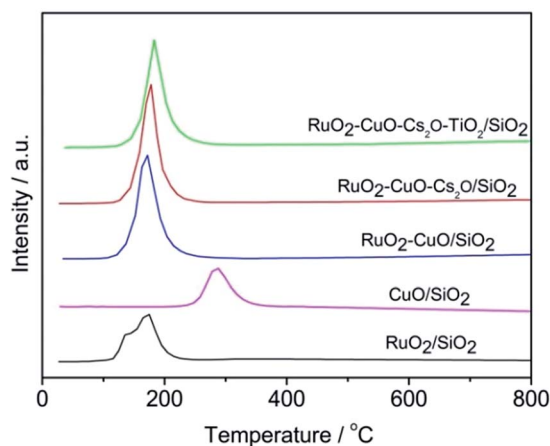
parameters could be performed to further maximize the PO production rate and to predict the best operating conditions for the RuO_2–CuO–Cs_2O–TiO_2/SiO_2 catalyst. But since many thousands of experiments would be needed to do so, the Box–Behnken design, a frequently employed optimization tool, was used in our study. Box–Behnken designs allow efficient estimation of the best conditions for complex, multi-variable experiments by manipulating a limited number of data points throughout a range of options.[36] A subset of the effects Box–Behnken predicts these four operating parameters should have on PO formation rate is illustrated in Fig. 9 (see detailed results in Table S1;† the PO selectivity and propylene conversion are shown in Fig. S1 and S2,† respectively). The full ranges of conditions were: 190–310 °C, 0.4–20.0 for O_2/C_3H_6 volume ratio, 0.03–0.33 for $(O_2 + C_3H_6)$/He volume ratio, and 30–70 cm³ min⁻¹ for the total feed flow rate.

The images displayed in Fig. 9a–c show the effects of reaction temperature varied with O_2/C_3H_6 volume ratio, $(O_2 + C_3H_6)$/He volume ratio, and total feed gas flow rate, respectively. Fig. 9a and b indicate that the PO formation rate was optimized at reaction temperatures around 250–290 °C when the O_2/C_3H_6 volume ratio was above ~16 or below ~3.5 and when the $(O_2 + C_3H_6)$/He volume ratio was above 0.20. Fig. 9c indicates that the total feed gas flow rate was optimized around 30–40 cm³ min⁻¹. Moreover, increasing the total feed gas flow rate results in a lower PO formation rate (Fig. 9c) due to a reduction in contact time with the catalyst. The images in Fig. 9d–f display the PO formation rates at a reaction temperature of 272 °C when varying $(O_2 + C_3H_6)$/He volume ratio vs. O_2/C_3H_6 volume ratio, total feed gas flow rate vs. O_2/C_3H_6 volume ratio, and total feed gas flow rate vs. $(O_2 + C_3H_6)$/He feed volume ratio, respectively. The most impactful variables on the PO formation rate are the O_2/C_3H_6 volume ratio and $(O_2 + C_3H_6)$/He volume ratio. Changing the total feed gas flow rate at the same $(O_2 + C_3H_6)$/He volume ratio (Fig. 9f) had less effect on PO formation than did changing the reaction temperature and O_2/C_3H_6 ratio. The highest predicted PO formation rate was >3000 g_{PO} h⁻¹ kg_{cat}⁻¹ at O_2/C_3H_6 volume ratio of above ~16 or below ~3.5, $(O_2 + C_3H_6)$/He volume ratio of above ~0.2, total feed gas flow rate of 30–40 cm³ min⁻¹, and the reaction temperature of 272 °C.

To confirm the predicted value of the optimal PO formation rate from the Box–Behnken design experiment, the previously ascertained process conditions were experimentally employed in catalytic performance testing (see Table S2†). Remarkably, under the selected testing condition (the reaction temperature of 272 °C, the O_2/C_3H_6 volume ratio of 3.1, the $(O_2 + C_3H_6)$/He volume ratio of 0.26, and the total feed gas flow rate of 34 cm³ min⁻¹) the highest experimental PO formation rate was 3015 g_{PO} h⁻¹ kg_{cat}⁻¹ (7.1% PO selectivity and 40.1% propylene conversion). To the best of our knowledge, this PO formation rate is the highest ever reported for the direct gas-phase epoxidation of propylene to PO under atmospheric pressure using only O_2 (see Fig. S3 and Table S3†), about 8 times higher than the best catalyst reported in the literature. The maximum PO selectivity was also ascertained using a similar procedure. The predicted conditions included a reaction temperature of 219 °C, O_2/C_3H_6 volume ratio of 4.1, the $(O_2 + C_3H_6)$/He volume ratio of
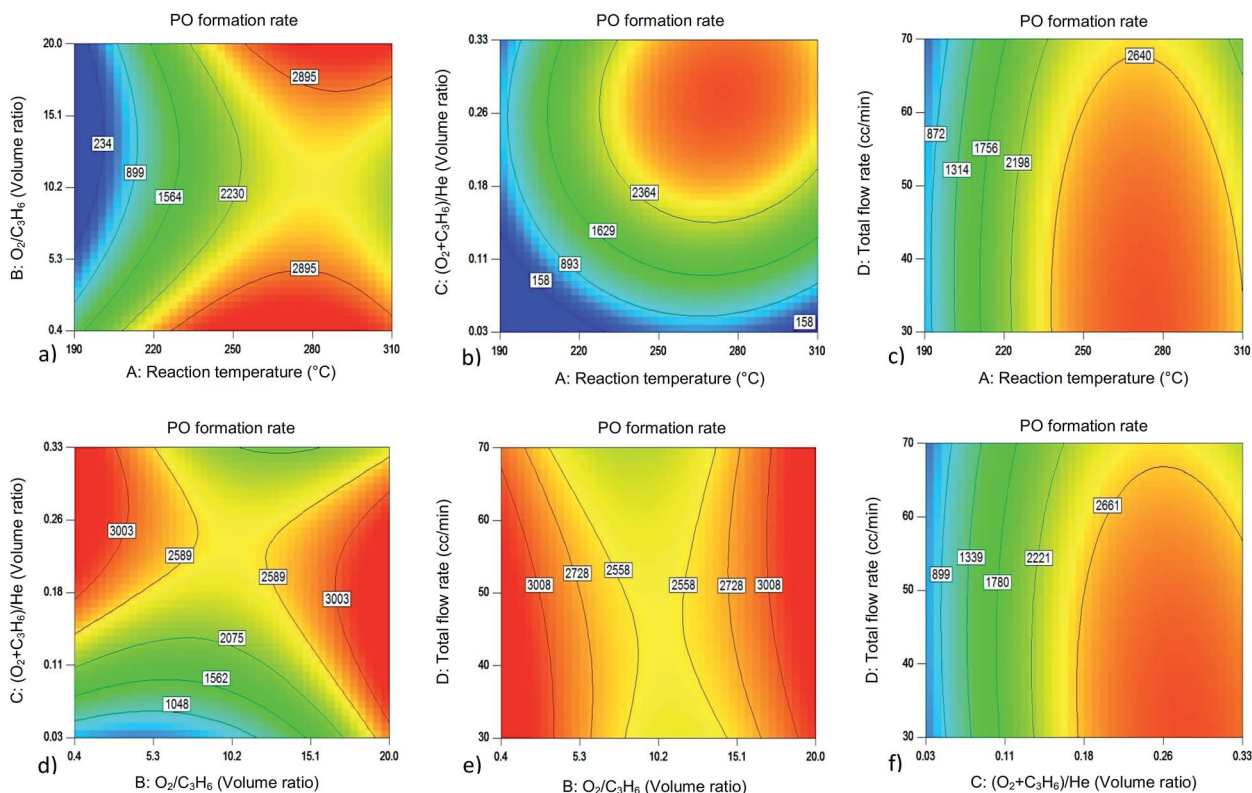

Fig. 8 H_2-TPR profiles of all combinations of RuO_2, CuO, Cs_2O, and TiO_2 on SiO_2. Each catalyst has wt% of Ru, Cu, Cs and/or Ti on SiO_2 of 12.59%, 6.29%, 0.91%, and 1.21%, respectively.

Fig. 9 (a)–(f) Contour plots showing PO formation rate (g_{PO} h^{-1} kg_{cat}^{-1}) from all combinations of 4 operating parameters; (a) A vs. B, (b) A vs. C, (c) A vs. D, (d) B vs. C, (e) B vs. D, (f) C vs. D; where A = reaction temperature (190–310 °C), B = O_2/C_3H_6 volume ratio (0.4–20.0), C = ($O_2 + C_3H_6$)/He volume ratio (0.03–0.33), and D = total feed gas flow rate (30–70 cm^3 min^{-1} by using He as balance gas). When two parameters were studied, A, B, C and/or D were fixed at 272 °C, 3.1, 0.26, and/or 34 cm^3 min^{-1}, respectively. Weight ratio of Ru/Cu/Cs/Ti/SiO$_2$ = 12.59/6.29/0.91/1.21/79, total metal loading on SiO$_2$ = 21 wt%.

0.32, and total feed gas flow rate of 70 cm^3 min^{-1}. The PO selectivity was 38.4% (1.3% propylene conversion and 573 g_{PO} h^{-1} kg_{cat}^{-1} for the PO formation rate). All of the results obtained from the experiments were in good agreement with the predicted values from the design experiment, i.e. less than ±3% error.

Since catalyst reusability is essential, a multiple test of the optimal catalyst with the optimal operating condition for PO formation rate was performed. Fig. 10 (also see Table S4†) charts PO selectivities and propylene conversions with PO formation rates of the optimal catalyst with and without treating with fumed HCl for 6 runs. Note that the data were collected 30 min into each run under the optimal condition. After the 6 times of using the catalyst, the activity for PO production decreased, particularly the PO formation rates and the propylene conversions, from 3015 g_{PO} h^{-1} kg_{cat}^{-1} with 40.1% of propylene conversion to 732 g_{PO} h^{-1} kg_{cat}^{-1} with 5.8% propylene conversion, indicating that the catalyst had a deactivation problem. This behavior was similar to the RuO$_2$–CuO–NaCl/SiO$_2$ catalysts previously reported in which the loss of Cl from the catalysts' surface resulted in deactivation.[15] It should be noted that Cl remaining on the surface comes from the RuCl$_3$ precursor. An investigation using SEM-EDS, comparing the fresh catalyst with the same catalyst after 6 runs, confirmed that the overall Cl content decreased (see Fig. S4†). Therefore, the

used catalyst was treated with fumed HCl. As seen in Fig. 10, the catalyst treated with fumed HCl after every run showed activity remarkably close to that of the fresh catalyst. Even after 6 runs, the activity for PO production was virtually unchanged,
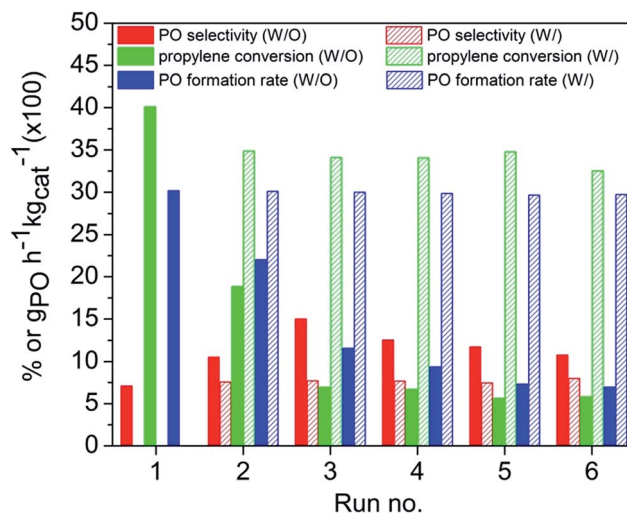

Fig. 10 Multiple test runs of the optimal RuO$_2$–CuO–Cs$_2$O–TiO$_2$/SiO$_2$ catalyst with (w/) and without (w/o) treating with fumed HCl under the optimal operating condition for PO formation rate.

indicating that the treatment with fumed HCl restores catalytic performance.

Conclusion

Catalysts based on RuO₂–CuO/SiO₂ were modified with Cs₂O and TiO₂ for the direct gas-phase epoxidation of propylene to PO using only O₂ under atmospheric pressure. Catalytic performance was first optimized by varying the weight percentage of Cs₂O in the RuO₂–CuO/SiO₂ catalyst and by varying the weight percentage of TiO₂ added to the best of those RuO₂–CuO–Cs₂O/SiO₂ catalysts. The multi-metallic catalyst performed best at weight ratios of Ru/Cu/Cs/Ti = 8.3/4.2/0.6/0.8 at a total metal loading of 21 wt%. Further optimization of the PO formation rate was pursued using the Box–Behnken design of experiments, varying the reaction temperature, O_2/C_3H_6 volume ratio, $(O_2 + C_3H_6)/He$ volume ratio, and total feed gas flow rate simultaneously. The highest PO formation rate and PO selectivity over the RuO₂–CuO–Cs₂O–TiO₂ catalyst were achieved at 3015 g_{PO} h^{-1} kg$_{cat}$$^{-1}$ and 38.4%, respectively, representing the highest PO formation rate ever reported for the title reaction. The characterizations of the optimal catalyst using XRD, XPS, NH₃-TPD, CO₂-TPD, SEM, and H₂-TPR technique revealed that the main active site for PO formation was the close proximity between crystalline RuO₂ and CuO where the synergy effect takes place. Cs₂O and TiO₂ acted as promoters by modulating the acidity or the basicity of RuO₂–CuO/SiO₂ surfaces. The catalyst exhibited a deactivation due to the loss of Cl. However, it can be recovered by treating with fumed HCl.

Acknowledgements

References

1 T. A. Nijhuis, M. Makkee, J. A. Moulijn and B. M. Weckhuysen, *Ind. Eng. Chem. Res.*, 2006, **45**, 3447–3459.
2 A. Prieto, M. Palomino, U. Díaz and A. Corma, *Catal. Today*, 2014, **227**, 87–95.
3 K. L. Ring and M. deGuzman, *Chemical Economics Handbook: Propylene Oxide*, IHS Chemical, 2016.
4 S. J. Khatib and S. T. Oyama, *Catal. Rev.*, 2015, **57**, 306–344.
5 J. Gaudet, K. K. Bando, Z. Song, T. Fujitani, W. Zhang, D. S. Su and S. T. Oyama, *J. Catal.*, 2011, **280**, 40–49; J. Chen, S. J. A. Halin, E. A. Pidko, M. W. G. M. Verhoeven, D. M. P. Ferrandez, E. J. M. Hensen, J. C. Schouten and T. A. Nijhuis, *ChemCatChem*, 2013, **5**, 467–478; W. S. Lee, M. Cem Akatay, E. A. Stach, F. H. Ribeiro and W. Nicholas Delgass, *J. Catal.*, 2013, **308**, 98–113; X. Feng, X. Duan, G. Qian, X. Zhou, D. Chen and W. Yuan, *Appl. Catal., B*, 2014, **150–151**, 396–401; X. Feng, X. Duan, J. Yang, G. Qian, X. Zhou, D. Chen and W. Yuan, *Chem. Eng. J.*, 2015, **278**, 234–239; M. Du, J. Huang, D. Sun and Q. Li, *Appl. Surf. Sci.*, 2016, **366**, 292–298; F. Jin, Y. Wu, S. Liu, T.-H. Lin, J.-F. Lee and S. Cheng, *Catal. Today*, 2016, **264**, 98–108.
6 K. Murata, Y. Liu, M. Inaba and N. Mimura, *Catal. Today*, 2004, **91–92**, 39–42; N. Mimura, S. Tsubota, K. Murata, K. K. Bando, J. J. Bravo-Suarez, M. Haruta and S. T. Oyama, *Catal. Lett.*, 2006, **110**, 47–51; F. Sun and S. Zhong, *J. Nat. Gas Chem.*, 2006, **15**, 45–51; S. Park, K. M. Cho, M. H. Youn, J. G. Seo, J. C. Jung, S.-H. Baeck, T. J. Kim, Y.-M. Chung, S.-H. Oh and I. K. Song, *Catal. Commun.*, 2008, **9**, 2485–2488; W.-S. Lee, M. Cem Akatay, E. A. Stach, F. H. Ribeiro and W. Nicholas Delgass, *J. Catal.*, 2012, **287**, 178–189.
7 S. Kalyoncu, D. Duzenli, I. Onal, A. Seubsai, D. Noon, S. Senkan, Z. Say, E. Vovk and E. Ozensoy, *Catal. Lett.*, 2015, **145**, 596–605.
8 E. Ananieva and A. Reitzmann, *Chem. Eng. Sci.*, 2004, **59**, 5509–5517; Q. Zhang, Q. Guo, X. Wang, T. Shishido and Y. Wang, *J. Catal.*, 2006, **239**, 105–116; S. Yang, W. Zhu, Q. Zhang and Y. Wang, *J. Catal.*, 2008, **254**, 251–262; Z. X. Song, N. Mimura, S. Tsubota, T. Fujitani and S. T. Oyama, *Catal. Lett.*, 2008, **121**, 33–38; J. Q. Lu, X. M. Zhang, J. J. Bravo-Suarez, T. Fujitani and S. T. Oyama, *Catal. Today*, 2009, **147**, 186–195; V. I. Sobolev and K. Y. Koltunov, *Appl. Catal., A*, 2014, **476**, 197–203.
9 E. A. Carter and W. A. Goddard, *J. Catal.*, 1988, **112**, 80–92.
10 R. M. Lambert, F. J. Williams, R. L. Cropley and A. Palermo, *J. Mol. Catal. A: Chem.*, 2005, **228**, 27–33.
11 L. J. Yang, J. L. He, Q. H. Zhang and Y. Wang, *J. Catal.*, 2010, **276**, 76–84.
12 D. Torres, N. Lopez, F. Illas and R. M. Lambert, *Angew. Chem., Int. Ed.*, 2007, **46**, 2055–2058.
13 X. Zheng, Q. Zhang, Y. Guo, W. Zhan, Y. Guo, Y. Wang and G. Lu, *J. Mol. Catal. A: Chem.*, 2012, **357**, 106–111.
14 A. Seubsai, M. Kahn and S. Senkan, *ChemCatChem*, 2011, **3**, 174–179.
15 A. Seubsai and S. Senkan, *ChemCatChem*, 2011, **3**, 1751–1754.
16 A. Miller, B. Zohour, A. Seubsai, D. Noon and S. Senkan, *Ind. Eng. Chem. Res.*, 2013, **52**, 9551–9555.
17 A. Seubsai, D. Noon, T. Chukeaw, B. Zohour, W. Donphai, M. Chareonpanich and S. Senkan, *J. Ind. Eng. Chem.*, 2015, **32**, 292–297.
18 J. He, Q. Zhai, Q. Zhang, W. Deng and Y. Wang, *J. Catal.*, 2013, **299**, 53–66.
19 X. Yang, S. Kattel, K. Xiong, K. Mudiyanselage, S. Rykov, S. D. Senanayake, J. A. Rodriguez, P. Liu, D. J. Stacchiola and J. G. Chen, *Angew. Chem., Int. Ed.*, 2015, **54**, 11946–11951.
20 J. Lu, M. Luo, H. Lei and C. Li, *Appl. Catal., A*, 2002, **237**, 11–19.
21 M. F. Luo, J. Q. Lu and C. Li, *Catal. Lett.*, 2003, **86**, 43–49; O. P. H. Vaughan, G. Kyriakou, N. Macleod, M. Tikhov and

R. M. Lambert, *J. Catal.*, 2005, **236**, 401–404; B. Zohour, D. Noon, A. Seubsai and S. Senkan, *Ind. Eng. Chem. Res.*, 2014, **53**, 6243–6248.

22 W. M. Zhu, Q. H. Zhang and Y. Wang, *J. Phys. Chem. C*, 2008, **112**, 7731–7734.

23 W. G. Su, S. G. Wang, P. L. Ying, Z. C. Feng and C. Li, *J. Catal.*, 2009, **268**, 165–174.

24 A. Seubsai, B. Zohour, D. Noon and S. Senkan, *ChemCatChem*, 2014, **6**, 1215–1219.

25 D. Duzenli, E. Seker, S. Senkan and I. Onal, *Catal. Lett.*, 2012, **142**, 1234–1243.

26 J. Q. Lu, M. F. Luo, H. Lei, X. H. Bao and C. Li, *J. Catal.*, 2002, **211**, 552–555; W. G. Su, S. G. Wang, P. L. Ying, Z. C. Feng and C. Li, *J. Catal.*, 2009, **268**, 165–174; X. Zheng, Q. Zhang, Y. Guo, W. Zhan, Y. Guo, Y. Wang and G. Lu, *J. Mol. Catal. A: Chem.*, 2012, **357**, 106–111; W. Long, Q. Zhai, J. He, Q. Zhang, W. Deng and Y. Wang, *ChemPlusChem*, 2012, **77**, 27–30.

27 K. Zhang, C. H. Chew, G. Q. Xu, J. Wang and L. M. Gan, *Langmuir*, 1999, **15**, 3056–3061.

28 K. Min, L. Tong Tao, C. Hao, Z. Sheng Mao, Z. Li Li and Z. Yu Xin, *Nanotechnology*, 2015, **26**, 304002.

29 S.-J. Yang and C. W. Bates, *Appl. Phys. Lett.*, 1980, **36**, 675–677.

30 R. Sanjines, H. Tang, H. Berger, F. Gozzo, G. Margaritondo and F. Levy, *J. Appl. Phys.*, 1994, **75**, 2945–2951.

31 Y. Lei, X. Chen, C. Xu, Z. Dai and K. Wei, *J. Catal.*, 2015, **321**, 100–112.

32 W. Yao, G. Lu, Y. Guo, Y. Guo, Y. Wang and Z. Zhang, *J. Mol. Catal. A: Chem.*, 2007, **276**, 162–167; G. Jin, G. Lu, Y. Guo, Y. Guo, J. Wang, W. Kong and X. Liu, *J. Mol. Catal. A: Chem.*, 2005, **232**, 165–172.

33 Z. L. Wang, Q. S. Liu, J. F. Yu, T. H. Wu and G. J. Wang, *Appl. Catal., A*, 2003, **239**, 87–94.

34 S. Galvagno, C. Crisafulli, R. Maggiore, G. R. Tauszik and A. Giannetto, *J. Therm. Anal.*, 1985, **30**, 611–618.

35 S. Anniballi, F. Cavani, A. Guerrini, B. Panzacchi, F. Trifirò, C. Fumagalli, R. Leanza and G. Mazzoni, *Catal. Today*, 2003, **78**, 117–129; Y. Xiaojiang, Y. Fumo and D. Lin, in *Advances in Energy Equipment Science and Engineering*, CRC Press, 2015; E. Sheerin, G. K. Reddy and P. Smirniotis, *Catal. Today*, 2016, **263**, 75–83.

36 S. L. C. Ferreira, R. E. Bruns, H. S. Ferreira, G. D. Matos, J. M. David, G. C. Brandão, E. G. P. da Silva, L. A. Portugal, P. S. dos Reis, A. S. Souza and W. N. L. dos Santos, *Anal. Chim. Acta*, 2007, **597**, 179–186.